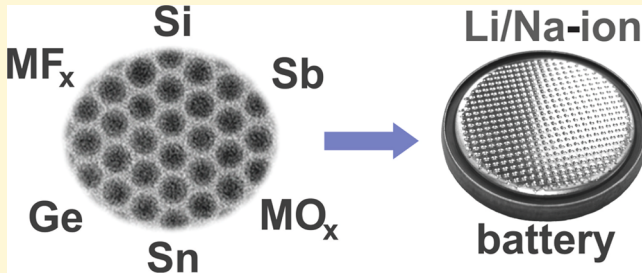


# Precisely Engineered Colloidal Nanoparticles and Nanocrystals for Li-Ion and Na-Ion Batteries: Model Systems or Practical Solutions?<sup>†</sup>

Marek F. Oszajca, Maryna I. Bodnarchuk, and Maksym V. Kovalenko\*

Institute of Inorganic Chemistry, Department of Chemistry and Applied Biosciences, ETH Zürich, CH-8093 Zürich, Switzerland  
Laboratory for Thin films and Photovoltaics, Empa – Swiss Federal Laboratories for Materials Science and Technology, CH-8600 Dübendorf, Switzerland

**ABSTRACT:** In recent years, the search for new electrode materials for rechargeable Li-ion batteries has undergone a drastic shift toward nanomaterials. A similar tendency is expected to occur for the conceptually similar Na-ion batteries. Due to very short internal diffusion paths, nanoscale materials are far less limited by their ionic or electronic conductivities than their bulk counterparts. Nanomaterials can also withstand much greater mechanical deformation during charge/discharge cycling. Overall, these favorable effects significantly enlarge the variety of inorganic compounds that can be used as Li and Na ion storage media. Herein, we discuss the perspectives of a specific family of nanomaterials—monodisperse colloidal nanocrystals and nanoparticles—for controlling and studying the effects of size, composition, and morphology on electrochemical properties. Despite clear scientific advantages, commercialization of such nanomaterials is presently hampered by their high cost of synthesis, owing to the use of organic solvents and coordination compounds.



## INTRODUCTION

Lithium(Li)-ion batteries (LIBs) remain the most widespread rechargeable electrochemical energy storage technology,<sup>1</sup> with tremendous importance for portable electronics as well as for the rapidly growing sector of environmentally benign electrical mobility (e-mobility).<sup>2</sup> The key advantages of commercial LIBs include long operation life, up to several thousand charging cycles, and the tunable balance between energy density and power density (often presented as a Ragone plot).<sup>3</sup> The major benefits of e-mobility are the reduction of CO<sub>2</sub> emissions and the more efficient use of energy due to the high efficiency of electric motors combined with regenerative breaking. A common fact for large cities is that roughly 50% of all trips by cars are shorter than 5 km. Within this distance, up to 5 times more hydrocarbons, 2–3 times more nitrogen oxides, and 10% more CO<sub>2</sub> are emitted than in the period after the engine has fully warmed up. Large, stationary batteries can provide backup power and stabilization for electrical grids. Globally, rechargeable batteries can help in reducing the human contribution to climate change by integrating electrical energy from renewable sources and by improving the efficiency of nonrenewable energy processes. Despite commercial success, there are several factors which still limit the competitiveness of LIBs in the aforementioned applications. Portable electronics benefit from any, even incremental, improvement in gravimetric and volumetric energy density. E-mobility is perhaps the most demanding application of LIBs and for becoming fully competitive with internal combustion engines requires increasing the energy density by a factor of 2–3, while

maintaining long cycling life and safety.<sup>4</sup> Stationary batteries for large-scale energy storage would require a 5- to 10-fold reduction of the battery cost and, therefore, call for cheaper post-Li-ion technologies such as sodium(Na)-ion batteries (SIBs).

In this Perspective, we discuss the scientific reasons underlying the presently strong focus on nanostructured materials as alternative, high-energy-density electrode materials for LIBs and SIBs. In particular, we focus on precisely engineered colloidal nanocrystals (NCs) and nanoparticles (NPs) as some of the best-defined nanomaterials that may help us to better understand and control the effects of the size, shape, surface chemistry, and composition on the electrochemical characteristics of electrode materials. We discuss a broad range of inorganic compounds that may become usable as high-energy-density cathode or anode materials due to the fact that, comparing to their bulk counterparts, nanoscopic materials are far less limited by their ionic and electronic conductivities and can withstand much larger volumetric changes. We also highlight the shortcomings of high surface-to-volume ratios and high porosities, and, for overcoming these effects, we outline a promising strategy of assembling the nanocomposite electrodes using secondary particles composed of monodisperse NCs and NPs. We show that despite bringing unique scientific insights and enhancing electrochemical performance, these nanomaterials presently cannot be

Received: May 14, 2014

Revised: September 2, 2014

Published: September 8, 2014

<sup>†</sup>This Perspective is part of the *Up-and-Coming* series.



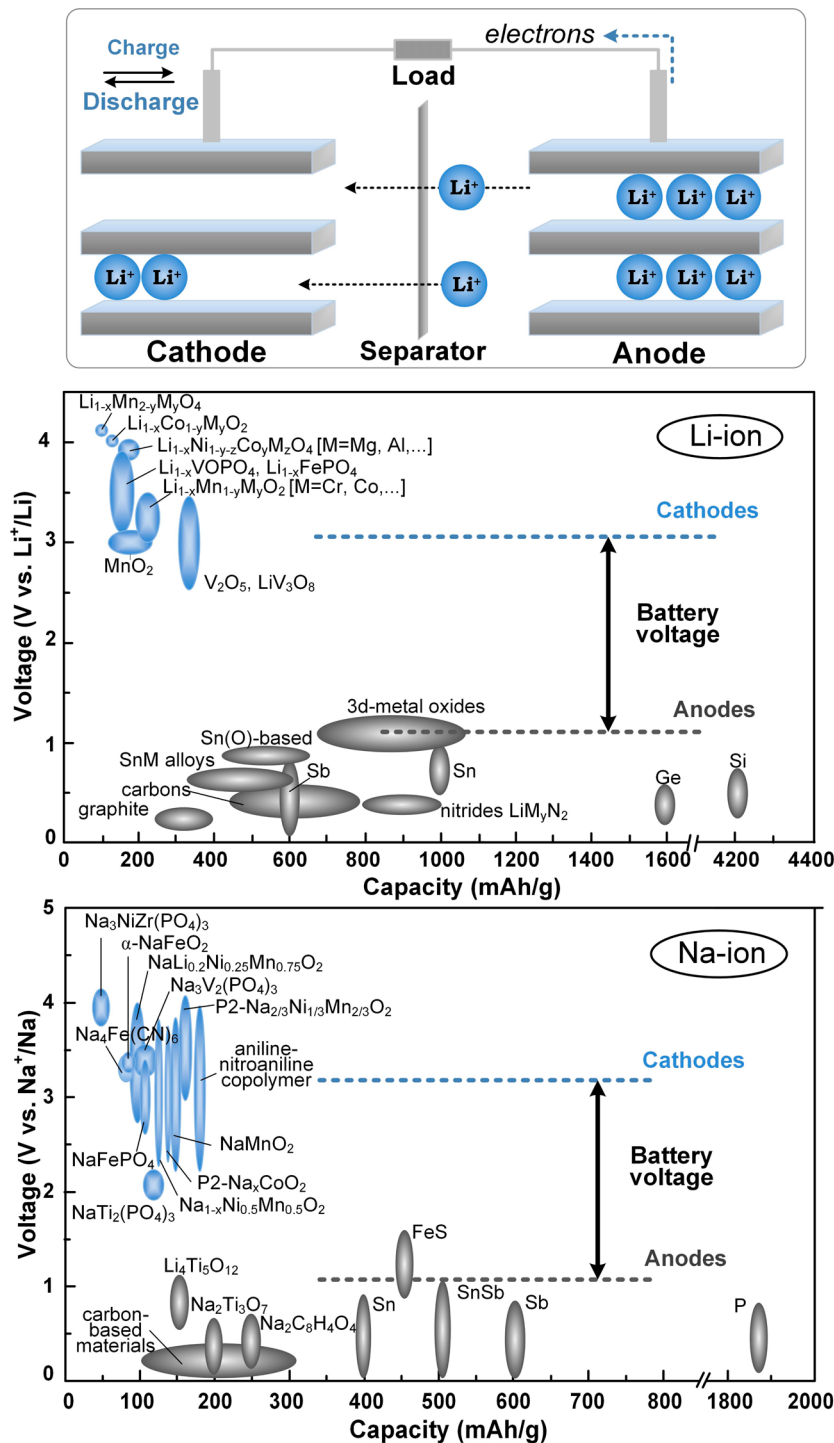


**Figure 1.** (top) Schematic principle of a Li-ion battery; (middle, bottom) capacities of known Li-ion and Na-ion electrode materials.

commercialized due to their high cost of synthesis requiring organic solvents and coordination compound precursors. For the nanocrystal research community, to which this Perspective article is primarily addressed, we provide an introduction into the basics of LIBs and SIBs and raise awareness of the potentially strong and unique link between nanocrystals and the field of batteries. In addition, we highlight the importance of unbiased and correct reporting of the performance metrics, allowing comparison between various materials and across publications.

## ■ HOW DOES A LI-ION BATTERY WORK?

The working principle of LIBs (and SIBs) is illustrated in Figure 1. Electrical energy can be converted into stored chemical energy (charge) and vice versa (discharge) by driving redox reactions at the electrode materials. Nonaqueous, electrochemically stable electrolyte such as a solution of LiPF<sub>6</sub> in alkyl carbonates is used for transporting Li<sup>+</sup> ions between the two electrodes, whereas electrons migrate via an external circuit. The difference in the electrochemical potential between the two electrode materials provides the theoretical voltage of a battery (V, Figure 1). The charge storage capacity

of an electrode material ( $C$ ), in gravimetric ( $\text{A h g}^{-1}$ ) or volumetric ( $\text{A h cm}^{-3}$ ) units, is determined by the ability of the material to uptake a significant amount of Li ions. Gravimetric charge storage capacity is often named **specific capacity** and is most commonly reported in units of  $\text{mA h g}^{-1}$ . A total charge storage capacity of a battery is determined by both the cathode and the anode ( $C_{\text{total}} = C_A C_C / (C_A + C_C)$ ). The product of  $V \times C$  provides the energy density ( $\text{W h g}^{-1}$ ). The theoretical capacities of the electrode materials presently dominating the market are  $135 \text{ mA h g}^{-1}$  for  $\text{LiCoO}_2$  cathodes (or  $170 \text{ mA h g}^{-1}$  for  $\text{LiFePO}_4$ ) and  $372 \text{ mA h g}^{-1}$  for graphite anodes.

The theoretical gravimetric and volumetric capacities for most commonly studied LIB electrode materials are presented in Figures 1 and 2. One can clearly see that the advantages of

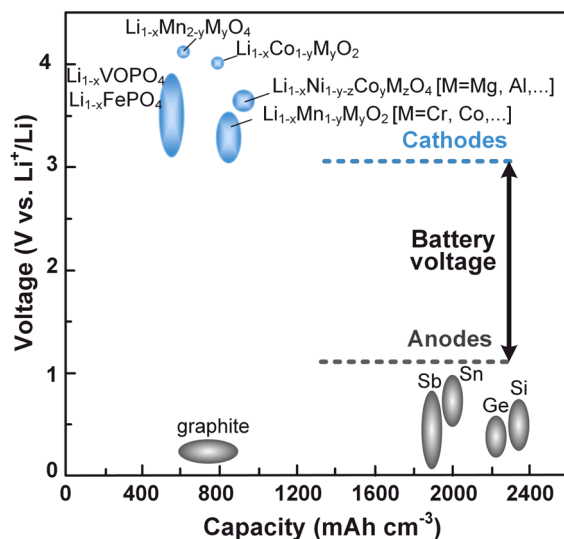


**Figure 2.** Theoretical volumetric capacities of major Li-ion electrode materials.

high-specific-capacity anode materials such as Sn and Si are usually offset in a volumetric representation (Figure 2). Alternative electrode materials have not only to possess higher specific capacities than graphite or  $\text{LiCoO}_2$  but also satisfactory retention of the capacity over the long-term and under fast charge/discharge cycling (high current densities). Safe operation under variable environmental conditions is equally important. The transition from commercial graphite anodes to the most intensely studied alternatives such as Si, Sn, and some metal oxides, with up to 10 times higher theoretical capacities ( $3579 \text{ mA h g}^{-1}$  for  $\text{Si} \leftrightarrow \text{Li}_5\text{Si}_4$  being the highest), is primarily hampered by the structural instabilities caused by drastic volumetric changes of 150–300% upon full lithiation to, e.g.,  $\text{Li}_3\text{Sb}$ ,  $\text{Li}_{15}\text{Si}_4$ ,  $\text{Li}_{15}\text{Ge}_4$ , and  $\text{Li}_{22}\text{Sn}_5$ <sup>5</sup> or by slow reaction kinetics. Theoretical values for volumetric changes can be estimated from the difference in the molar volumes ( $\%V_m$ ) between the final ( $\text{Li}_x\text{M}$ ) and initial metallic ( $\text{M}$ ) phases:  $\Delta V = 100\% \times [V_m(\text{Li}_x\text{M}) - V_m(\text{M})]/V_m(\text{M})$ . At present, immense research efforts are focused on nanostructuring of the active material in order to mitigate the effects of volumetric changes and to enhance the kinetics of the conversion or alloying reactions.<sup>1,2,6</sup> Analysis of the available literature shows that while LIB anodes are on a fast track to higher performance due to the availability of materials with high theoretical capacities of  $1000 \text{ mA h g}^{-1}$  and above (Si, Sn, and Ge), the Achilles' heel of LIBs is still the cathode.

## ■ ON THE OPTIMAL REPORTING OF PERFORMANCE METRICS

The operation of a rechargeable battery is characterized by several standard performance metrics which are, however, often incoherently presented in the literature. Therefore, a clear definition of such metrics would be very useful, especially for new researchers in this field. The careful adherence to agreed-upon standards is crucial for a reliable comparison of the results obtained in different research groups. It also aids the external community (e.g., engineers, investors, or the general public) to properly assess the competing claims. Cherry-picking of the data, along with insufficient description of the experimental procedures, can irreversibly damage the research field and mislead future researchers. Similar problems in the field of organic photovoltaics (OPVs) have been recently discussed by Luber and Buriak,<sup>7</sup> who showed a simple method for statistical treatment of the power conversion efficiencies of OPV cells allowing an unbiased comparison of the results. We suggest that the same approach for obtaining statistically significant reporting is also applicable for analyzing battery cells and should at least be applied to **charge storage capacity** (discussed above)—the most important attribute of an electrode material. The capacity is the value by which different materials are often compared, and extreme care must be made when reporting capacities close to or (increasingly frequently and often erroneously) above the theoretical values. We note that a standard certification of the performance of an electrode material by an independent, internationally recognized institution is not available to scientists in this field, contrary to that for photovoltaic cells which are routinely certified by institutions such as the National Renewable Energy Laboratory, Newport, or Fraunhofer ISE, etc.

The **cycling stability** (e.g., capacity retention vs number of cycles) and the **rate-capability** (capacity retention vs charge/discharge current rates) are highly dependent on the mass loading of an active material (in  $\text{mg cm}^{-2}$ ) and porosity. For practical purposes, such as in the comparison of prototype or commercial cells, areal capacity (in  $\text{mA h cm}^{-2}$ ) is often more relevant than specific capacity. For example, a typical LIB used in electric vehicles consists of current collectors, electrodes, electrolyte, separators, binders, and additives, in which the active electrode material constitutes roughly 40–50% by mass.<sup>8</sup> In commercial batteries, the areal capacity typically lies in the range of 2–3.5  $\text{mA h cm}^{-2}$ . Further to this end, presenting the electrochemical data for cells with very low loadings of active material is suitable for scientific assessment but not for assessing the commercial applicability since the capacity usually does not remain constant with increasing electrode thickness.<sup>9</sup> Therefore, in addition to reporting the specific capacity and its cycle retention, the mass loading and thickness (or tap density) of the electrode should also be reported, especially because these quantities are easily measurable.

The electrochemical testing conditions may also affect the observed performance. The majority of galvanostatic cycling measurements presented in the scientific literature are, in fact, conducted in half-cells, via cycling vs Li foil as a reference electrode. Metallic Li is known to form dendrites during electroplating when current densities go above  $0.5\text{--}1 \text{ mA cm}^{-2}$ .<sup>10</sup> Consequently, in order to prevent the significant influence of Li foil on the performance of a working electrode, especially during long-term cycling, the cycling tests should be conducted at sufficiently low current densities by adjusting the

mass-loading. The charge and discharge rates are often expressed as *C-rates*, which is defined as 1C for a charge or discharge occurring during 1 h and  $nC$  for faster cycles of  $1/n$  hours. The corresponding current density is determined by the theoretical capacity. Thus, a clarification of which theoretical capacity is taken in this calculation should be provided. For instance, if the theoretical specific capacity for a Si anode is considered to be 3579 mA h g<sup>-1</sup>, the 0.5C-rate corresponds to a current density of 1789.5 mA g<sup>-1</sup>. The portable electronics demands cells with a cycle life of at least 300–1000 cycles, whereas batteries for electrical vehicles may be required to possess an order of magnitude longer cycling life. Another crucial parameter reflecting battery performance is *Coulombic efficiency (CE)*, which is the ratio between the amounts of electricity spent for the delithiation and lithiation processes. During the first cycle, the CE is typically low due to the formation of the solid–electrolyte interfacial (SEI) layer, an electrochemical side process that passivates the electrode; in the subsequent cycles, the CE should be above 99.9% in well-optimized commercial cells. For further discussion of the considerations related to correct measuring, reporting, and comparison of the performance of electrochemical cells, refer to the recent review article by Nitta and Yushin.<sup>10</sup>

### ■ Na-ION BATTERY AS A FUTURE ALTERNATIVE

A conceptually identical technology, the SIB, is emerging as a viable alternative due to the much greater natural abundance and more even distribution of Na reserves as compared to Li.<sup>11</sup> Large-scale SIBs can secure the supply of renewable energy through the buffering of intermittent resources such as wind and solar energy, in stationary installations close to the respective power plants. In comparison to LIBs, there is an even greater need for efficient Na ion anode materials since silicon does not reversibly store Na ions at ambient conditions,<sup>12</sup> graphite shows negligible capacities of 30–35 mA h g<sup>-1</sup>,<sup>13</sup> and other carbonaceous materials exhibit capacities of less than 300 mA h g<sup>-1</sup> at rather low current rates and suffer from low tap density due to high porosity.<sup>1</sup> Present-day SIB cathodes are approaching the performance of LIB cathodes.<sup>6a,b,14</sup> Figure 1 shows nearly all of the materials that have been tested as cathode and anode materials in SIBs and have demonstrated reversible charging for at least several cycles. The general trend is similar to that of LIBs; polyanionic metal salts may be used as cathodes with charge storage capacities not exceeding 200 mA h g<sup>-1</sup>, while on the anode side, the most promising materials are those containing antimony (Sb) and phosphorus (P). Currently, phosphorus-based anodes exhibit the highest capacities, reaching 1890 mA h g<sup>-1</sup> (the theoretical value is 2596 mA h g<sup>-1</sup> for the formation of Na<sub>3</sub>P),<sup>15</sup> but with poor capacity retention. The second best (Sb) is characterized by lower capacities of up to 640 mA h g<sup>-1</sup> (the theoretical value is 660 mA h g<sup>-1</sup>) but shows superior cycling stability and rate capability.<sup>16</sup>

In comparison to LIBs which have a history of more than 20 years of research and development, there are 100 times fewer publications related to SIBs and 90% of them were published in the last 3 years. We must note that there are no scientific reasons to assume that SIBs should not reach or even surpass the performance of the LIB counterparts. Sodium has a very suitable redox potential ( $E_{\text{Na}/\text{Na}^+} = -2.70$  V vs SHE), only ~0.3 V below that of  $E_{\text{Li}/\text{Li}^+}$ . Sodium has a larger ionic radius than Li (1.16 vs 0.9 Å), which leads to interesting differences in solid-state chemistry. For example, while the synthesis of LiFeF<sub>3</sub> is

unknown, NaFeF<sub>3</sub> is a highly stable compound and a promising cathode material.<sup>17</sup> Additionally, DFT calculations have shown that the activation energy for Na ion diffusion in layered oxide electrodes or in solid electrolytes may be even lower than that for Li ion diffusion.<sup>18</sup> Furthermore, the diffusivity of Na ions in liquid electrolytes is essentially identical to that of Li ions. The lack of research on SIBs until the 2010s can be attributed to the successful commercialization of LIBs since the 1990s, and only recently rising concerns about the availability of lithium for the increased production of car batteries and for large-scale battery applications have led to the increased research activity.

### ■ WHAT CAN NANOSTRUCTURING OFFER TO LIBS/SIBS?

The past decade has seen intense research on nanostructured cathodes and anodes for LIBs.<sup>19</sup> Nanostructuring has revived a tremendous interest in a large number of the alternative cathode and anode materials that, despite their ability to store large quantities of Li ions, were previously discarded on the basis of their poor electronic or ionic conductivity, slow reaction kinetics, or large volumetric changes. Size reduction dramatically reduces the path for mass and charge transport and mitigates the volumetric changes during electrode operation, as outlined in Figure 3. As an example, highly electronically insulating LiFePO<sub>4</sub> became a practical cathode material and was eventually commercialized only after its mean primary

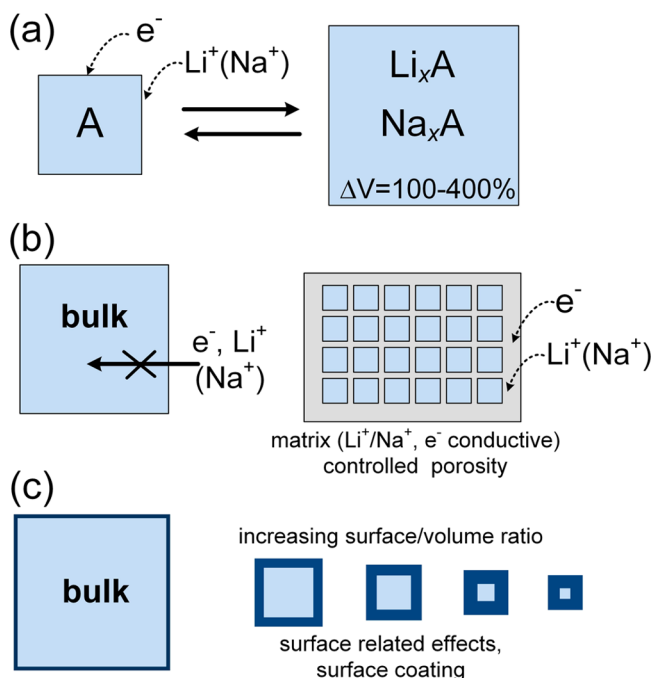


**Figure 3.** Major effects of downsizing on the electrochemical performance of electrode materials. (a) Volumetric changes associated with insertion and removal of the alkali ions become less detrimental and better accommodated; (b) poor ionic/electronic conductors become usable when prepared as a nanocomposite in a conductive matrix; (c) increased surface-to-volume ratio improves the kinetics of Li/Na insertion/removal, enhances other surface-related phenomena (e.g., modifies electrochemical potential), and allows efficient interfacing with other components or surface coating. However, detrimental processes such as excessive consumption of electrolytes for the formation of SEI layer and reactions of electrode materials with electrolytes are often enhanced as well.

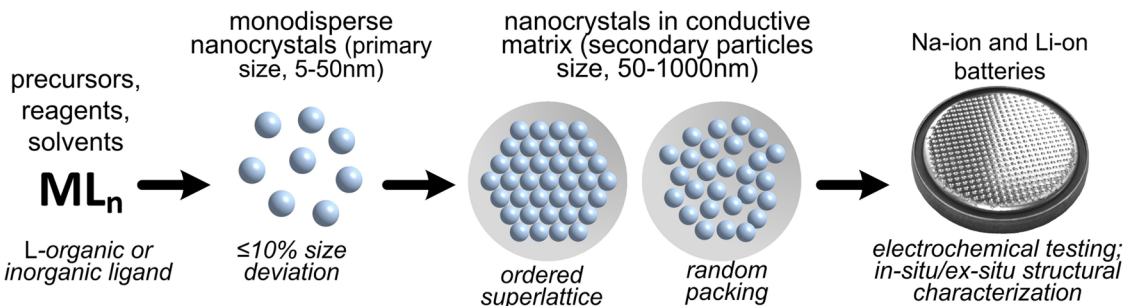


**Figure 4.** Generalized bottom-up strategy for constructing LIB/SIB electrodes using colloidal NPs and NCs as building blocks and secondary particles as a mean to reduce the amount of SEI and to stabilize it.

crystallite size was reduced to below 100 nm and by combination with a conductive coating or mixing with conductive additive. The smaller the reaction zone, the lower is the kinetic constraint for conversion and alloying reactions.<sup>20</sup> With respect to alloying anode materials (e.g., Sn, Si, and Ge), several reports have shown evidence for the existence of a critical size below which the fracture of a particle may not occur.<sup>21</sup> Furthermore, small particle size allows efficient mixing of the active electrode material with other components such as the conductive carbon additive (usually 30–100 nm NPs of amorphous carbon). In addition, the colloidal stability and homogeneity of slurries, e.g., dispersions of active material, additive, and binder in a solvent, is far greater for nanoscale particles than for microscale counterparts.

The diffusion time constant is given by the square of the diffusion length ( $L$ ) divided by the diffusion constant ( $D$ ).

$$\tau = \frac{L^2}{D} \quad (1)$$

Consequently, much higher rate-capabilities are commonly observed for nanoscale electrodes than in conventional microcrystalline powders.<sup>16,22</sup> Investigations of size effects on ionic transport within the active material and through the electrolyte constitute an emerging field of nanoionics.<sup>23</sup>

Very high surface-to-volume ratios can have positive as well as detrimental effects. A large specific surface area enables efficient conductive surface coating and/or interfacing with other electrode components. Carbon coating or sandwiching between graphene layers (commonly, reduced graphene oxide) are among the simplest and most efficient approaches to maintaining high electronic connectivity while preventing the aggregation of active particles.<sup>24</sup> High surface curvature and surface tension can significantly alter the chemical potential of the electrode by up to 100 mV<sup>25</sup> and can cause deviation from flat voltage plateau behavior in the charge/discharge curves.<sup>26</sup> The high surface area can, however, also enhance various side reactions between the electrode material and the electrolyte, such as in the corrosion and dissolution of transition metal oxides. Most importantly, the high specific surface area of nanomaterials leads to a high, irreversible capacity loss in the first cycle due to a large amount of SEI formed in the first cycle and the fact that the SEI layer itself becomes increasingly unstable with increasing surface area and curvature. Additionally, higher porosity reduces the overall volumetric energy density of the electrodes.

## ■ COLLOIDAL NANOPARTICLES AND NANOCRYSTALS AS ELECTRODE MATERIALS

The development of monodisperse colloidal NCs, that is, a nanoparticle ensemble with a standard size deviation below 10%, was initially driven by tremendous interest in quantum-size effects, observed in semiconductor NCs as small as 2–10 nm in diameter. Early in the 1990s, the methodology based on surfactant-assisted colloidal synthesis in nonpolar organic solvents was proposed for CdSe<sup>27</sup> and later extended to many other metals, metal oxides, metal halides, and common inorganic compounds.<sup>28</sup> A detailed discussion of the synthesis of monodisperse NCs can be found elsewhere.<sup>28a,c</sup> The selection of appropriate molecular precursors is critically important, which ideally need to be soluble in nonpolar organic solvents, stable, liquid or solid at room temperature, sufficiently reactive at elevated temperatures, and not involved in undesired side reactions with the capping ligands and solvents and must yield the target inorganic material in high purity. It is also very helpful if the precursor is commercially available or has well documented and simple preparation methods. The methodology of colloidal synthesis also requires the ability to independently tune the rate of nucleation and growth of NCs/NPs. In particular, fast nucleation followed by slower growth from oversaturated solutions favors the formation of monodisperse NCs and can be achieved, for instance, via the rapid injection of the precursors into a hot solvent. The resulting shape of the NCs/NPs is determined by a complex interplay between the underlying crystal structure and the growth conditions. Thus, the addition of surfactants and their mixtures is necessary to control the nucleation and growth kinetics, as well as to adjust the shape of the resulting NCs/NPs. Presently, great research efforts are focused on the solid-state device applications of monodisperse NCs, mainly in optoelectronics (e.g., photovoltaics, light-emitting devices, photodetectors, field-effect transistors, etc.).<sup>28a,29</sup> *The excellent size-, shape-, and compositional-tunability of colloidal NPs and NCs may also open new “degrees of freedom” in battery research.* An unambiguous structure–property relationship can be provided with uniform nanomaterials, contrary to the vast majority of nanocomposites in the literature, such as those produced in aqueous solutions by coprecipitation or by high-energy ball milling, with broad and inhomogeneous size and morphology distributions. All three effects summarized in Figure 3 can thus also be accurately related to the mean particle size and morphology. We should also emphasize that many electrodes that are not formulated as nanostructured do become nanostructured during electrochemical cycling. For instance, metal oxides or fluorides reversibly form metallic NPs,

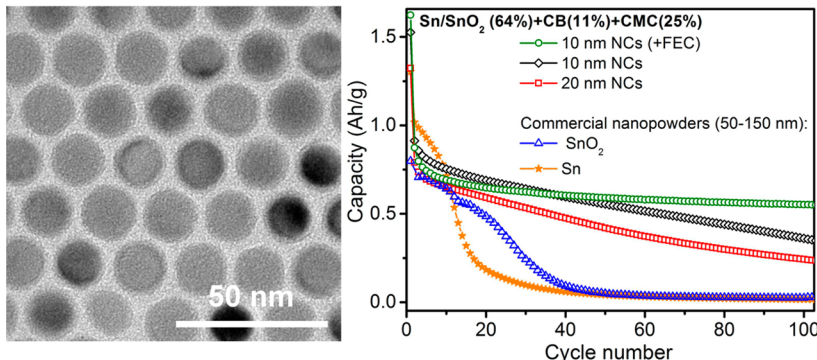


**Figure 5.** (left) TEM image of colloidally synthesized Sn/SnO<sub>2</sub> NCs; (right) reversible discharge capacities of anodes comprising commercial Sn and SnO<sub>2</sub> nanopowders and colloidally synthesized Sn/SnO<sub>2</sub> NCs (current density 1 A g<sup>-1</sup>). Reproduced with permission from ref 37. Copyright 2013 American Chemical Society.

often as small as a few nanometers, during conversion reactions, such as in  $MF_x + Li + e^- \leftrightarrow M + LiF$ .<sup>30</sup> Therefore, research on conversion materials may greatly benefit from the deployment of uniform and small nanoparticles as starting materials, instead of as rather poorly defined nanocomposites obtained by high-energy ball-milling.

In Figure 4, we envisage a strategy for producing battery electrodes comprising monodisperse NCs as an active material. While commonly employed industrial synthesis techniques involve high-energy mechanical grinding, uniform NCs can be produced from molecular precursors. Before NCs can be integrated into the actual electrode, the protective monolayer of capping molecules (ligands and surfactants) must be removed or displaced by conductive species using mild chemical treatments in order to preserve the integrity of the NCs.<sup>31</sup> For materials with high thermal stability such as iron oxide, thermally induced carbonization of the ligands into a thin conductive layer of carbon is also very practical and convenient.<sup>32</sup>

## ■ SECONDARY PARTICLES

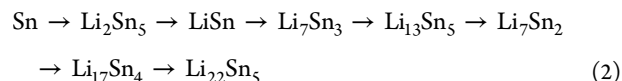
As suggested in Figure 4, colloidal NCs may be conveniently arranged into secondary particles, thus reducing the overall active material–electrolyte and electrode–electrolyte interfacial areas. This may lead to the reduced reactivity of the active material toward the electrolyte due to the physical separation between them and may lower the amount of and increase the stability of the SEI. The latter effect is particularly important for alloying/conversion electrode materials. This would reduce the irreversible capacity loss at the first cycle and would lead to higher Coulombic efficiencies and higher cycling stabilities. Within the secondary particle, efficient electronic and ionic transport can be provided by, for instance, embedding NCs into a conductive carbon matrix. Several recent reports have shown an elegant methodology for the formation of such secondary particles using the unique ability of monodisperse NPs/NCs to form long-range ordered assemblies (superlattices) upon solvent evaporation.<sup>28a,b</sup> In order to obtain secondary particles of 50–1000 nm in size, droplets of nonpolar solvents such as toluene or chloroform (“oil droplets”) containing NPs/NCs are dispersed in a polar solvent such as water by adding surfactants, forming an “oil-in-water” type microemulsion. Slow evaporation of the volatile nonpolar solvent leads to the formation of uniformly sized aggregates of NPs/NCs (secondary particles), with very dense periodic (superlattices) or random packing within each aggregate.<sup>33</sup> This approach, combined with thermal

carbonization of the ligands, has been recently deployed for the construction of Fe<sub>3</sub>O<sub>4</sub>/carbon nanocomposites.<sup>34</sup> Subsequent polyvinylpyrrolidone coating followed by pyrolysis yields a thin and continuous amorphous carbon layer on the exterior of the secondary particle. The potential benefits of the periodic superlattice packing include a well-defined interparticle spacing and a high volumetric packing density of 74% for fcc or hcp packing in single component assemblies or 50–80% for binary component mixtures. Recent studies have shown that NCs arranged into superlattices are much more resistant to sintering, compared to disordered packing,<sup>35</sup> which might be important during the carbonization step. We would also like to highlight two reports in which highly ordered and dense assemblies of MnO<sup>36</sup> and Fe<sub>3</sub>O<sub>4</sub> or MnFe<sub>2</sub>O<sub>4</sub> NCs<sup>32c</sup> within an amorphous carbon matrix were obtained in a single step simply by thermal decomposition of the corresponding metal oleates. More specifically, during continuous heating from room temperature to 500 °C, the metal oleate first served as a solvent, wherein by self-decomposition it generated metal oxide NPs followed by the carbonization of all oleate groups. In addition to these examples with colloidal NCs, the formation of secondary particles has been demonstrated in other systems such as in pomegranate-inspired composites in which Si particles were embedded in voids that were specifically designed within the conductive carbon matrix.<sup>38</sup>

## ■ EXAMPLES OF COLLOIDAL NCs AS ELECTRODE MATERIALS

We note that there have been only very few reports dealing with monodisperse NCs and NPs as battery electrode materials, mainly as anode materials, leaving ample room for future work by the nanocrystal research community.

Tin exhibits a volumetric expansion of up to 300% during the formation of Li<sub>22</sub>Sn<sub>5</sub> (specific capacity of 992 mA h g<sup>-1</sup>). The lithiation of Sn requires transitions through six intermediate crystalline phases:<sup>10,39</sup>



This complex sequence of crystalline phases is believed to be the reason for the increased fracturing of tin, which leads to reduced cycling stability. In fact, a recent report shows that Sn NCs as small as 10 nm still undergo extensive mechanical damage during lithiation.<sup>40</sup> Kravchik et al.<sup>37</sup> have shown a pronounced size effect on the electrochemical performance of

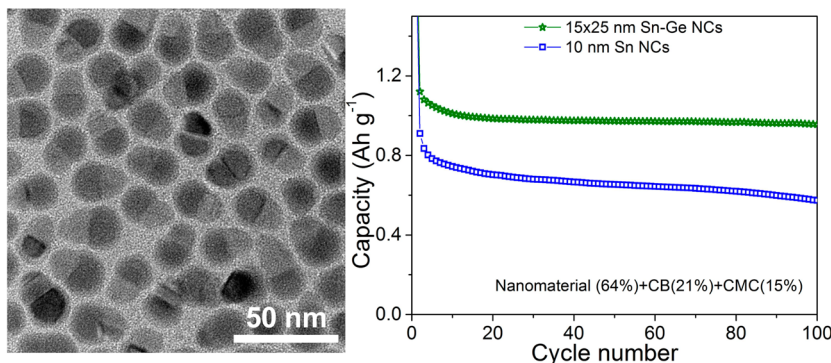


**Figure 6.** (left) TEM image of colloidally synthesized Sn–Ge nanocrystals; (right) reversible discharge capacities of the anodes comprising Sn–Ge and Sn NCs in Li-ion half-cells (current density is 1 A g<sup>-1</sup>). Reproduced with permission from ref 43. Copyright 2014 American Chemical Society.

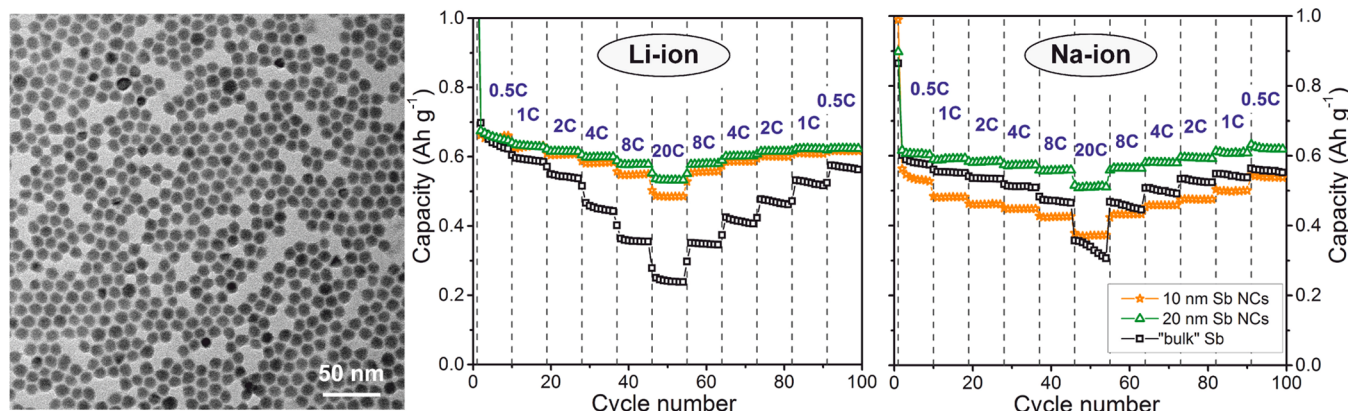


**Figure 7.** TEM image of colloidally synthesized ~10 nm Sb NCs; rate capability tests of anodes containing Sb NCs in Li-ion and Na-ion half cells (1C = 0.66 A g<sup>-1</sup>, 64% of active material). Reproduced with permission from ref 16. Copyright 2014 American Chemical Society.

Sn NCs covered with a layer of native oxide (Sn/SnO<sub>2</sub> core–shell NCs): only 10 nm NCs could retain a capacity above 700 mA h g<sup>-1</sup> after 100 cycles of deep charging (0.005–2 V) at a relatively high current of 1000 mA g<sup>-1</sup> (Figure 5). Fluoroethylenecarbonate (FEC) as the electrolyte additive for stabilizing the SEI<sup>6b</sup> was also necessary for achieving satisfactory cycling stability.

Compositional modulation within the NCs provides another powerful tool to control electrochemical response. From the perspective of Li-alloying anodes, the creation of a Sn–Ge nanocomposite could realize the best characteristics of both elements. Metallic Sn can impart an enhanced electronic conductivity, while Ge can increase the overall capacity to at least 1000 mA h g<sup>-1</sup>. The theoretical specific capacity of Ge is still debated, with the most conservative estimate being 1384 mA h g<sup>-1</sup> for conversion to Li<sub>15</sub>Ge<sub>4</sub>.<sup>41</sup> In Ge, the room temperature Li ionic diffusivities were reported to be 400 and 6000 times higher than in Si and Sn, respectively,<sup>42</sup> and its electronic conductivity is at least a factor of 10<sup>4</sup> higher than that of Si. Hence, highly stable and fast cycling have been recently reported for nanoparticulate Ge, exhibiting capacities of 700 mA h g<sup>-1</sup> through 500 cycles at a charge/discharge rate of 10C.<sup>5</sup> Since Sn and Ge are nearly immiscible in the bulk, colloidal Sn–Ge nanoheterodimers (Figure 6)<sup>43</sup> perhaps serve as ultimately the most homogeneous and uniform Sn–Ge mixture. Such efficient mixing with well-defined crystallite size of each component can hardly be achieved with top-down methods such as mechanical milling.<sup>5</sup> Synergistic effects, reported for Sn–Ge nanorod heterostructures (Figure 6),<sup>43</sup>

include a high charge storage capacity above 1000 mA h g<sup>-1</sup> at a relatively high current density of 1 A g<sup>-1</sup> and improved cycling stability. The former is provided by Ge, whereas the latter can be explained by the stepwise lithiation of Sn and Ge at different electrochemical potentials.

Antimony is a viable alternative to Sn and had been much less explored than Sn, Ge, and Si. Although it has a considerably lower theoretical specific capacity (660 mA h g<sup>-1</sup> for conversion to Li<sub>3</sub>Sb) than Si and Sn, the volumetric capacities are very similar: 1890 mA h cm<sup>-3</sup> for Sb, 2200 mA h cm<sup>-3</sup> for Si, and 2000 mA h cm<sup>-3</sup> for Sn. All three have specific capacities that are still much higher than that of graphite (843 mA h cm<sup>-3</sup>).<sup>44</sup> Several advantageous properties have prompted recent work on Sb-based anodes. Antimony is of semimetallic nature and hence the electronic conductivity is optimal for electrode operation. Its crystalline structure is characterized by a low atomic packing factor of 39%,<sup>44</sup> and, therefore, complete lithiation only leads to a moderate volumetric change of 135%, considerably smaller than that of Si (310%) and Sn (260%). The crystal structure of hexagonal Sb is comprised of puckered large channels for the diffusion of alkali ions. Moreover, during lithiation it forms only one intermediate phase (Li<sub>2</sub>Sb); delithiation directly yields elemental Sb.<sup>44,45</sup> This is very different from Sn, discussed above, in which multiple phase transformations between crystalline phases may slow down the overall reaction kinetics. Together, these peculiarities improve the kinetics of Li-ion insertion and extraction and allow the deployment of bulk microcrystalline Sb as an electrode material with close to theoretical capacity.<sup>46</sup> Finally, and perhaps most importantly,

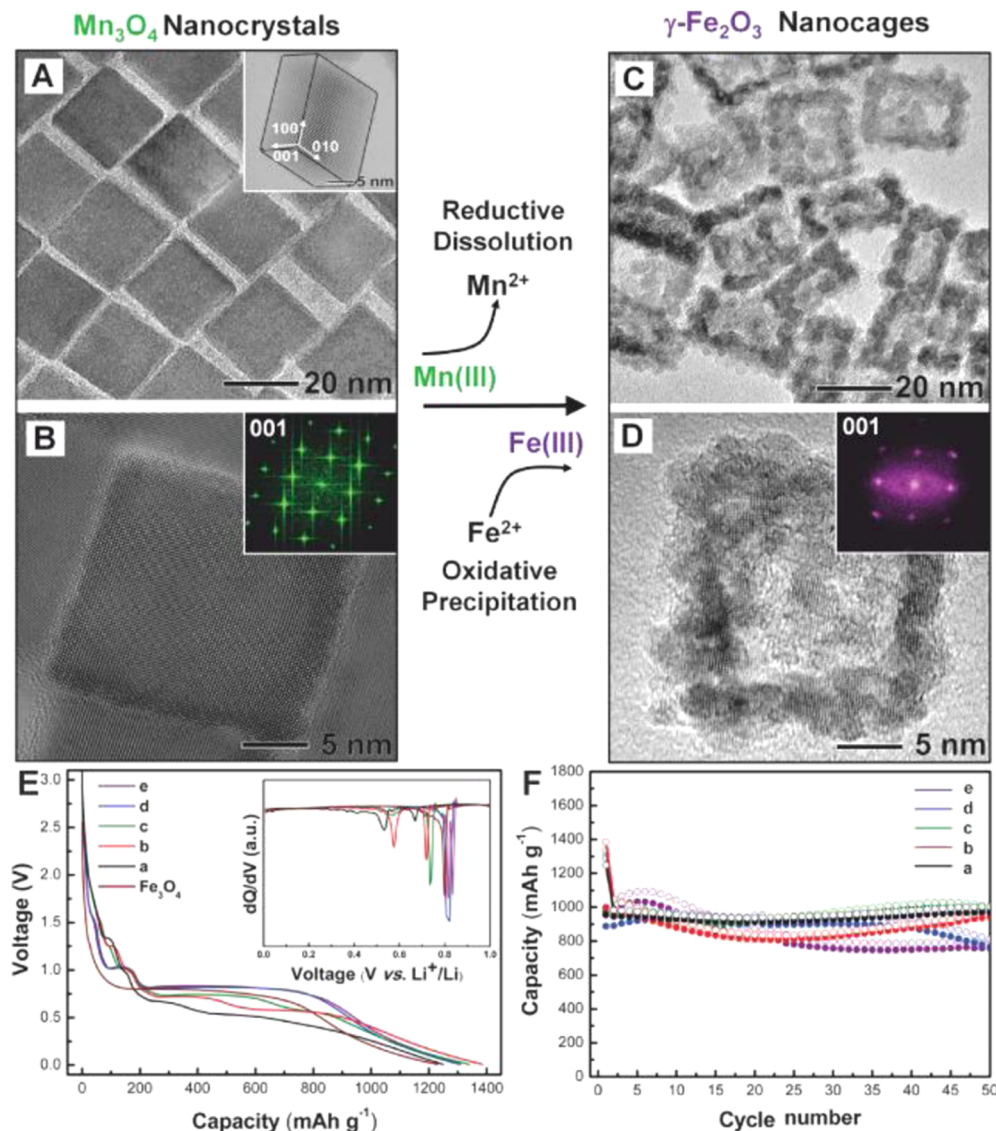


**Figure 8.** (A) TEM image of Mn<sub>3</sub>O<sub>4</sub> NCs. The inset shows the corresponding HRTEM image of a single NC recorded along the [111] axis. (B) HRTEM image of a single Mn<sub>3</sub>O<sub>4</sub> NC recorded along the [001] axis. The inset shows the corresponding FT pattern. (C) TEM and (D) HRTEM image of the γ-Fe<sub>2</sub>O<sub>3</sub> nanocages. The inset shows the corresponding FT pattern. (E) First discharge curves (F) and cycle performances of carbon-coated hollow Mn<sub>3-x</sub>Fe<sub>x</sub>O<sub>4</sub> NCs: (a) Mn<sub>2.0</sub>Fe<sub>1.0</sub>O<sub>4</sub>, (b) Mn<sub>1.5</sub>Fe<sub>1.5</sub>O<sub>4</sub>, (c) Mn<sub>1.1</sub>Fe<sub>1.9</sub>O<sub>4</sub>, (d) Mn<sub>0.6</sub>Fe<sub>2.4</sub>O<sub>4</sub>, and (e) Mn<sub>0.3</sub>Fe<sub>2.7</sub>O<sub>4</sub>. Reprinted with permission from ref 53c. Copyright 2013 American Association for the Advancement of Science.

the insertion of Na ions into Sb is found to be just as efficient and as fast as for Li ions.<sup>46</sup> Recently, He et al.<sup>16</sup> have shown that the utilization of colloidally synthesized 10 and 20 nm Sb NCs with narrow size distributions of 7–11% (Figure 7) allows the construction of a SIB anode with exceptional rate capability and 85% retention of the initial capacity (580–640 mA h g<sup>-1</sup> at 0.5–1C) when cycled with a current density of 13.2 A g<sup>-1</sup> (20C rate, Figure 7).<sup>16</sup> Furthermore, Na-ion anodes were found to exhibit very similar cycling stability and rate-capability to those of LIB anodes despite a much larger %ΔV of 290% upon full sodiation to hexagonal Na<sub>3</sub>Sb. With a capacity retention of ca. 80% at high current rates of 20C (13.2 A g<sup>-1</sup>), nanoscale Sb is the best-performing Na-ion anode material identified so far and is comparable to the fastest Li-ion intercalation materials such as graphite<sup>47</sup> and lithium titanates.<sup>48</sup>

Studies of Si and Ge NPs as Li-ion storage media are also extensively reported in the literature. These NPs can be obtained more easily by gas-phase methods such as laser

pyrolysis than by colloidal synthesis methods.<sup>6c,22d,49</sup> An overall analysis of the literature shows that the major advantage of Si is still its high capacity, while the rate capability is systematically lower than that of Sn or Ge. Yushin et al. have used sodium alginate as a water-soluble binder and obtained the highly stable cycling of 30–50 nm Si NPs with capacities above 1000 mA h g<sup>-1</sup> at a current density of 1200 mA g<sup>-1</sup>.<sup>6c</sup> Ge NPs exhibit excellent rate capability, cycling stability, and a capacity above 1000 mA h g<sup>-1</sup>,<sup>22d</sup> but the raw material cost of Ge is prohibitively high (at present) for most applications. We would also like to point the reader's attention to reports concerning silicon nanowires (see the mini-review<sup>50</sup>), including those synthesized colloidally.<sup>51</sup> Wires provide an intrinsic advantage in terms of electronic transport within the active material and may serve as efficient current collectors and as Li-ion storage media at the same time. For example, without any conductive additive, Si nanowire electrodes were reported to exhibit capacities of over 2000 mA h g<sup>-1</sup> for 100 cycles at a rate of C/

10 and over 1200  $\text{mA h g}^{-1}$  when cycled more rapidly at 1C ( $1\text{C} = 3579 \text{ mA g}^{-1}$ ).<sup>51,52</sup>

The concept of precisely engineered colloidal nanomaterials has also been presented for transition metal oxides as electrode materials.<sup>22a,b,31b,32a,b,53</sup> Recently, Hyeon et al.<sup>53c</sup> have demonstrated the first example of galvanic replacement reaction in metal oxide NCs (Figure 8).  $\text{Mn}_3\text{O}_4$  nanocubes were converted into hollow  $\gamma\text{-Fe}_2\text{O}_3$  nanocages via cationic exchange accompanied by the reduction of Mn(III) by Fe(II). Interim products of this exchange were  $\text{Mn}_{3-x}\text{Fe}_x\text{O}_4$  nanocages that showed peculiar electrochemical properties. In particular, the average discharge voltages were tunable from 0.4 to 0.8 V vs  $\text{Li}^+/\text{Li}$  by increasing the proportion of Fe. The hollow morphology provided an extra free space to alleviate the volume changes, allowing stable cycling. Altering the  $x = \text{Mn}/\text{Fe}$  ratio also showed a pronounced effect on cycling stability, showing the best results for  $x = 1-2$ .

Contrary to anodes, there are few reports in the literature describing monodisperse colloidal NCs as cathode materials because polyanionic oxide NCs—typical cathode materials (Figure 1)—are usually produced in polydisperse form by coprecipitation under hydrothermal conditions. As an example of nonaqueous high-temperature synthesis,  $\text{LiMnPO}_4$  NCs were obtained in different shapes and sizes (from 7 nm spheres to 100 nm rods) using oleic acid and oleylamine as a surfactant–solvent medium.<sup>54</sup> After proper optimization of the surface chemistry (ligand removal and carbonization) the cathode capacity was measured to be 165  $\text{mA h g}^{-1}$  (97% of the theoretical capacity). Hollow iron oxide NCs, produced via the nanoscale Kirkendall effect upon the oxidation of Fe NCs, were studied as cathodes for Li- and Na-ion storage by Shevchenko et al. (Figure 9).<sup>53a,b</sup> During the formation of such NCs, a high

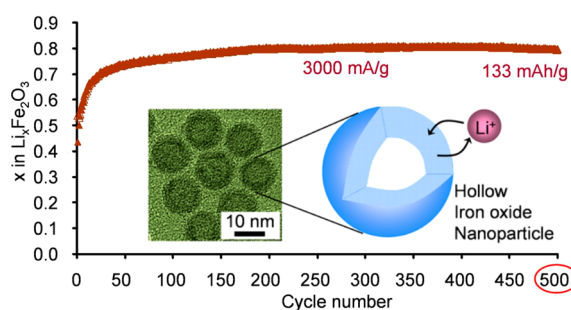


**Figure 9.** Rate performance of  $\gamma\text{-Fe}_2\text{O}_3$  NCs electrode operated for 500 cycles at a high current density of 3000  $\text{mA g}^{-1}$ , with delivering capacity of 133  $\text{mA h g}^{-1}$  via intercalation mechanism at high voltages (2.5–4.5 V). Reproduced with permission from ref 53a. Copyright 2012 American Chemical Society.

concentration of vacancies is generated which are, in turn, responsible for the formation of voids. The authors have posited as to the importance of these cation vacancies for the extensive and reversible intercalation of Li and Na ions at high voltages (ca. 1.35 Li or ~1.4 Na per  $\gamma\text{-Fe}_2\text{O}_3$  unit at 2.5–4.5 V, in the cathodic region).<sup>53a,b</sup> Importantly, the storage and transport of alkali ions occurs exclusively via intercalation, without noticeable conversion of the oxide into metallic Fe. The resulting electrodes were characterized by high cycling stability at elevated current density (3000  $\text{mA/g}$ ) with >99.5% CE and impressive capacities of up to 133  $\text{mA h g}^{-1}$  and 99  $\text{mA h g}^{-1}$  for Li and Na ions, respectively.

## PERSPECTIVE: MODEL SYSTEMS OR PRACTICAL SOLUTIONS?

The better defined the material is, the less biased is the interpretation of the results by the authors and the perception of them by the readers. For this reason, precisely engineered NCs can undoubtedly serve as excellent model systems. Much room remains to further advance the concepts reviewed herein, especially in terms of the control over the SEI layer stability and CE by the proper engineering of the secondary particle. These factors are crucial for securing the long cycling life of a battery (>1000 cycles) needed for commercial applications. We highlight that very little is known about the morphological and compositional evolution of these NCs and NPs during electrochemical cycling and future studies should expand the use of *in situ* methods (small- and wide-angle X-ray scattering, X-ray tomography, Raman spectroscopy, transmission electron microscopy, etc.).

At present, it is too early to consider colloidally synthesized, precisely engineered NPs and NCs as industrially applicable, due to the simple reality of high manufacturing costs. In order to reach the market, batteries based on these or other nanomaterials must be produced at a cost similar to the current Li-ion technology (300–800 \$/(kW h)).<sup>55</sup> This limits the price of the active material to  $\leq 100$  \$/kg, which is unrealistic for syntheses involving organic solvents, surfactants, and molecular precursors. As an example of a typical, inexpensive colloidal nanomaterial, the synthesis of 1 kg of PbS NCs produces roughly 1200 kg of waste, of which ~50% are solvents needed for material purification.<sup>56</sup> New and more economical synthetic routes have been developed, and the most studied example of CdSe NCs has subsequently experienced a 10-fold decrease in cost (from 570 \$  $\text{g}^{-1}$  to 58 \$  $\text{g}^{-1}$ ).<sup>56</sup> Upscaling in an industrial setting can further reduce the price by up to 1 order of magnitude, but not more. Hence the cost of colloidal nanomaterials is still roughly 2–3 orders of magnitude higher than is demanded for LIB/SIB applications. The complicated, costly, and lengthy synthesis of nanostructures is currently, in the opinion of many experts, the major bottleneck for their commercialization. For instance, Panasonic's first commercial 18650-type cell with a nanosilicon-based anode has not, until now, entered the market, although it was already expected in 2013.<sup>34</sup> *We therefore believe that, in the near-future, precise NC engineering will rather provide model systems for research purposes.* Yet this research will provide great predictive power due to its delivery of better understood structure–property relationships. As an example, it has been shown that Sn and Sb NCs have very different size-effects on cycling stability. While the performance of Sn NCs is strongly size-dependent and is satisfactory only at very small sizes of 10 nm or below, Sb NCs exhibit stable and near-theoretical capacity as long as their size is in the 20–100 nm range and, surprisingly, display significantly decreased capacities in particles smaller than 20 nm. This result suggests that inexpensive routes to Sb NCs, such as aqueous-based reduction methods, may lead to very practical performance as long as the produced polydisperse colloids fall into the target size range of 20–100 nm.

Although anode materials were mainly discussed, much more work still remains to be done on the cathode side of the battery. A simple calculation of the total capacity of a battery using  $C_{\text{total}} = C_A C_C / (C_A + C_C)$  shows that if the graphite anode of a battery is replaced with a higher capacity alternative (Sn, Ge, Si), keeping the same capacity of the typical cathode (below 140

$\text{mA h g}^{-1}$ ), the overall improvement will not be greater than 21% for Sn, 25% for Ge, and 32% for Si anodes (operated at their theoretical capacity). The challenge for the synthesis of cathode material NPs and NCs is that the compounds providing the highest energy density are based on multi-component oxides, containing three to four transition metals, such as  $\text{Li}[\text{Ni}_{0.8}\text{Co}_{0.1}\text{Mn}_{0.1}]\text{O}_2$  ( $200 \text{ mA h g}^{-1}$ ).<sup>57</sup> It might be very interesting to develop a precision synthesis of  $x\text{Li}_2\text{MnO}_3$ – $(1-x)\text{LiMO}_2$  ( $M = \text{Mn, Ni, or Co}$ ) in the form of uniform NCs with core–shell morphology (with  $\text{Li}_2\text{MnO}_3$  being the shell), as it has been previously shown that high capacities of  $250 \text{ mA h g}^{-1}$  are attainable only when  $\text{Li}_2\text{MnO}_3$  is coating the  $\text{LiMO}_2$  phase.<sup>58</sup> Another important class of highly promising cathodes materials is metal fluorides, such as  $\text{FeF}_2$  and  $\text{FeF}_3$ . These fluorides can deliver capacities of up to  $712 \text{ mA h g}^{-1}$  via conversion reactions:  $\text{FeF}_x + x\text{Li}^+ + xe^- \leftrightarrow \text{Fe} + x\text{LiF}$  ( $x = 2, 3$ ). As demonstrated by Amatucci et al. for high-energy milled samples, this conversion reaction becomes fully reversible only when the mean crystal size is reduced to ca. 10 nm or below.<sup>20</sup> Thus, the precision synthesis of such sub-10 nm metal fluoride particles may be highly advantageous for understanding and controlling kinetics of conversion reactions and is fully feasible from the perspective of inorganic chemistry.

## AUTHOR INFORMATION

### Corresponding Author

\*E-mail: mvkovalenko@ethz.ch.

### Author Contributions

The manuscript was prepared through contributions by all of the co-authors. All authors have given their approval to the final version of the manuscript.

### Notes

The authors declare no competing financial interest.

### Biography

Maksym Kovalenko has been a tenure-track Assistant Professor of Inorganic Chemistry at ETH Zürich since July 2011. His group is also partially hosted by EMPA (Swiss Federal Laboratories for Materials Science and Technology) to support his highly interdisciplinary research program. He completed graduate studies at Johannes Kepler University Linz (Austria, 2004–2007, with Prof. Wolfgang Heiss), followed by postdoctoral training at the University of Chicago (USA, 2008–2011, with Prof. Dmitri Talapin). His present scientific focus is on the development of new synthesis methods for inorganic nanomaterials, their surface chemistry engineering, and assembly into macroscopically large solids. His ultimate, practical goal is to provide novel inorganic materials for rechargeable Li-ion batteries, photovoltaics, and optoelectronics. He is the recipient of an ERC Starting Grant 2012 and Ruzicka Preis 2013.

## ACKNOWLEDGMENTS

We thank Nicholas Stadie for reading this manuscript. This work was financially supported by Swiss Federal Commission for Technology and Innovation (CTI) through CTI-Projekt Nr. 14698.2 PFIW-IW and by CTI Swiss Competence Centers for Energy Research (SCCER Heat and Electricity Storage).

## REFERENCES

- Palacin, M. R. *Chem. Soc. Rev.* **2009**, *38*, 2565–2575.
- Goodenough, J. B.; Kim, Y. *Chem. Mater.* **2009**, *22*, 587–603.
- Dang, C.; Lee, J.; Breen, C.; Steckel, J. S.; Coe-Sullivan, S.; Nurmikko, A. *Nat. Nanotechnol.* **2012**, *7*, 335–339.
- Hayner, C. M.; Zhao, X.; Kung, H. H. *Annu. Rev. Chem. Biomol. Eng.* **2012**, *3*, 445–471.
- Kim, M. G.; Cho, J. *J. Electrochem. Soc.* **2009**, *156*, A277–A282.
- (a) Magasinski, A.; Dixon, P.; Hertzberg, B.; Kvít, A.; Ayala, J.; Yushin, G. *Nat. Mater.* **2010**, *9*, 353–358. (b) Chockla, A. M.; Klavetter, K. C.; Mullins, C. B.; Korgel, B. A. *Chem. Mater.* **2012**, *24*, 3738–3745. (c) Kovalenko, I.; Zdyrko, B.; Magasinski, A.; Hertzberg, B.; Milicev, Z.; Burtovyy, R.; Luzinov, I.; Yushin, G. *Science* **2011**, *333*, 75–79. (d) Beattie, S. D.; Larcher, D.; Morcrette, M.; Simon, B.; Tarascon, J. M. *J. Electrochem. Soc.* **2008**, *155*, 158–163. (e) Chan, C. K.; Peng, H.; Liu, G.; McIlwrath, K.; Zhang, X. F.; Huggins, R. A.; Cui, Y. *Nat. Nanotechnol.* **2008**, *3*, 31–35. (f) Yoon, S.; Park, C.-M.; Sohn, H.-J. *Electrochem. Solid-State Lett.* **2008**, *11*, A42–A45.
- Luber, E. J.; Buriak, J. M. *ACS Nano* **2013**, *7*, 4708–4714.
- Dunn, J. B.; Gaines, L.; Barnes, M.; Sullivan, J.; Wang, M. <http://greet.es.anl.gov/files/lib-lca> (2012).
- Gogotsi, Y.; Simon, P. *Science* **2011**, *334*, 917–918.
- Nitta, N.; Yushin, G. *Part. Part. Syst. Charact.* **2014**, *31*, 317–336.
- Palomares, V.; Serras, P.; Villaluenga, I.; Hueso, K. B.; Carretero-Gonzalez, J.; Rojo, T. *Energy Environ. Sci.* **2012**, *5*, 5884–5901.
- Larcher, D.; Beattie, S.; Morcrette, M.; Edstrom, K.; Jumas, J.-C.; Tarascon, J.-M. *J. Mater. Chem.* **2007**, *17*, 3759–3772.
- Ge, P.; Fouletier, M. *Solid State Ionics* **1988**, 28–30 (Part 2), 1172–1175.
- Park, Y.-U.; Seo, D.-H.; Kwon, H.-S.; Kim, B.; Kim, J.; Kim, H.; Kim, I.; Yoo, H.-I.; Kang, K. *J. Am. Chem. Soc.* **2013**, *135*, 13870–13878.
- Kim, Y.; Park, Y.; Choi, A.; Choi, N.-S.; Kim, J.; Lee, J.; Ryu, J. H.; Oh, S. M.; Lee, K. T. *Adv. Mater.* **2013**, *25*, 3045–3049.
- He, M.; Kravchyk, K. V.; Walter, M.; Kovalenko, M. V. *Nano Lett.* **2014**, *14*, 1255–1262.
- Yamada, Y.; Doi, T.; Tanaka, I.; Okada, S.; Yamaki, J.-i. *J. Power Sources* **2011**, *196*, 4837–4841.
- Ong, S. P.; Chevrier, V. L.; Hautier, G.; Jain, A.; Moore, C.; Kim, S.; Ma, X.; Ceder, G. *Energy Environ. Sci.* **2011**, *4*, 3680–3688.
- (a) Bruce, P. G.; Scrosati, B.; Tarascon, J.-M. *Angew. Chem., Int. Ed.* **2008**, *47*, 2930–2946. (b) Wagemaker, M.; Mulder, F. M. *Acc. Chem. Res.* **2013**, *46*, 1206–1215.
- Wang, F.; Robert, R.; Chernova, N. A.; Pereira, N.; Omenya, F.; Badway, F.; Hua, X.; Ruotolo, M.; Zhang, R.; Wu, L.; Volkov, V.; Su, D.; Key, B.; Whittingham, M. S.; Grey, C. P.; Amatucci, G. G.; Zhu, Y.; Graetz, J. *J. Am. Chem. Soc.* **2011**, *133*, 18828–18836.
- (a) Liu, X. H.; Zhong, L.; Huang, S.; Mao, S. X.; Zhu, T.; Huang, J. Y. *ACS Nano* **2012**, *6*, 1522–1531. (b) Aifantis, K. E.; Haycock, M.; Sanders, P.; Hackney, S. A. *Mater. Sci. Eng., A* **2011**, *529*, 55–61.
- (a) Wang, H.; Cui, L.-F.; Yang, Y.; Casalongue, H. S.; Robinson, J. T.; Liang, Y.; Cui, Y.; Dai, H. *J. Am. Chem. Soc.* **2010**, *132*, 13978–13980. (b) Xu, X.; Cao, R.; Jeong, S.; Cho, J. *Nano Lett.* **2012**, *12*, 4988–4991. (c) Xu, Y.; Liu, Q.; Zhu, Y.; Liu, Y.; Langrock, A.; Zachariah, M. R.; Wang, C. *Nano Lett.* **2013**, *13*, 470–474. (d) Klavetter, K. C.; Wood, S. M.; Lin, Y.-M.; Snider, J. L.; Davy, N. C.; Chockla, A. M.; Romanovicz, D. K.; Korgel, B. A.; Lee, J.-W.; Heller, A.; Mullins, C. B. *J. Power Sources* **2013**, *238*, 123–136.
- Maier, J. *Chem. Mater.* **2014**, *26*, 348–360.
- (a) Li, N.; Song, H.; Cui, H.; Yang, G.; Wang, C. *J. Mater. Chem. A* **2014**, *2*, 2526–2537. (b) Yuan, F.-W.; Tuan, H.-Y. *Chem. Mater.* **2014**, *26*, 2172–2179. (c) Yu, W.-J.; Hou, P.-X.; Li, F.; Liu, C. *J. Mater. Chem. B* **2012**, *22*, 13756–13763.
- (a) Maier, J. *J. Power Sources* **2007**, *174*, 569–574. (b) Jamnik, J.; Maier, J. *Phys. Chem. Chem. Phys.* **2003**, *5*, 5215–5220.
- (a) Okubo, M.; Mizuno, Y.; Yamada, H.; Kim, J.; Hosono, E.; Zhou, H.; Kudo, T.; Honma, I. *ACS Nano* **2010**, *4*, 741–752. (b) Ganapathy, S.; Wagemaker, M. *ACS Nano* **2012**, *6*, 8702–8712.
- Murray, C. B.; Norris, D. J.; Bawendi, M. G. *J. Am. Chem. Soc.* **1993**, *115*, 8706–8715.

- (28) (a) Talapin, D. V.; Lee, J.-S.; Kovalenko, M. V.; Shevchenko, E. V. *Chem. Rev.* **2010**, *110*, 389–458. (b) Murray, C. B.; Kagan, C. R.; Bawendi, M. G. *Annu. Rev. Mater. Sci.* **2000**, *30*, 545–610. (c) Park, J.; Joo, J.; Kwon, S. G.; Jang, Y.; Hyeon, T. *Angew. Chem., Int. Ed.* **2007**, *46*, 4630–4660. (d) Park, J.; An, K. J.; Hwang, Y. S.; Park, J. G.; Noh, H. J.; Kim, J. Y.; Park, J. H.; Hwang, N. M.; Hyeon, T. *Nat. Mater.* **2004**, *3*, 891–895.
- (29) Kramer, I. J.; Sargent, E. H. *Chem. Rev.* **2013**, *114*, 863–882.
- (30) (a) Wiaderek, K. M.; Borkiewicz, O. J.; Pereira, N.; Ilavsky, J.; Amatucci, G. G.; Chupas, P. J.; Chapman, K. W. *J. Am. Chem. Soc.* **2014**, *136*, 6211–6214. (b) Wiaderek, K. M.; Borkiewicz, O. J.; Castillo-Martinez, E.; Robert, R.; Pereira, N.; Amatucci, G. G.; Grey, C. P.; Chupas, P. J.; Chapman, K. W. *J. Am. Chem. Soc.* **2013**, *135*, 4070–4078.
- (31) (a) Rosen, E. L.; Buonsanti, R.; Llordes, A.; Sawvel, A. M.; Milliron, D. J.; Helms, B. A. *Angew. Chem., Int. Ed.* **2011**, *51*, 684–689. (b) Buonsanti, R.; Pick, T. E.; Krins, N.; Richardson, T. J.; Helms, B. A.; Milliron, D. J. *Nano Lett.* **2012**, *12*, 3872–3877. (c) Kovalenko, M. V.; Bodnarchuk, M. I.; Zaumseil, J.; Lee, J.-S.; Talapin, D. V. *J. Am. Chem. Soc.* **2010**, *132*, 10085–10092. (d) Nag, A.; Kovalenko, M. V.; Lee, J.-S.; Liu, W.; Spokoyny, B.; Talapin, D. V. *J. Am. Chem. Soc.* **2011**, *133*, 10612–10620. (e) Talapin, D. V.; Murray, C. B. *Science* **2005**, *310*, 86–89.
- (32) (a) Lee, S. H.; Yu, S.-H.; Lee, J. E.; Jin, A.; Lee, D. J.; Lee, N.; Jo, H.; Shin, K.; Ahn, T.-Y.; Kim, Y.-W.; Choe, H.; Sung, Y.-E.; Hyeon, T. *Nano Lett.* **2013**, *13*, 4249–4256. (b) Lee, J. E.; Yu, S.-H.; Lee, D. J.; Lee, D.-C.; Han, S. I.; Sung, Y.-E.; Hyeon, T. *Energy Environ. Sci.* **2012**, *5*, 9528–9533. (c) Jang, B.; Park, M.; Chae, O. B.; Park, S.; Kim, Y.; Oh, S. M.; Piao, Y.; Hyeon, T. *J. Am. Chem. Soc.* **2012**, *134*, 15010–15015.
- (33) (a) Zhuang, J. Q.; Wu, H. M.; Yang, Y. A.; Cao, Y. C. *J. Am. Chem. Soc.* **2007**, *129*, 14166–14167. (b) Bai, F.; Wang, D. S.; Huo, Z. Y.; Chen, W.; Liu, L. P.; Liang, X.; Chen, C.; Wang, X.; Peng, Q.; Li, Y. D. *Angew. Chem., Int. Ed.* **2007**, *46*, 6650–6653.
- (34) Martin, C. *Nat. Nanotechnol.* **2014**, *9*, 327–328.
- (35) Dong, A.; Chen, J.; Ye, X.; Kikkawa, J. M.; Murray, C. B. *J. Am. Chem. Soc.* **2011**, *133*, 13296–13299.
- (36) Wang, T.; Peng, Z.; Wang, Y.; Tang, J.; Zheng, G. *Sci. Rep.* **2013**, *3*, 2693.
- (37) Kravchyk, K.; Protesescu, L.; Bodnarchuk, M. I.; Krumeich, F.; Yarema, M.; Walter, M.; Guntlin, C.; Kovalenko, M. V. *J. Am. Chem. Soc.* **2013**, *135*, 4199–4202.
- (38) Liu, N.; Lu, Z.; Zhao, J.; McDowell, M. T.; Lee, H.-W.; Zhao, W.; Cui, Y. *Nat. Nanotechnol.* **2014**, *9*, 187–192.
- (39) Courtney, I. A.; Dahn, J. R. *J. Electrochem. Soc.* **1997**, *144*, 2045–2052.
- (40) Xu, L.; Kim, C.; Shukla, A. K.; Dong, A.; Mattox, T. M.; Milliron, D. J.; Cabana, J. *Nano Lett.* **2013**, *13*, 1800–1805.
- (41) Baggetto, L.; Notten, P. H. L. *J. Electrochem. Soc.* **2009**, *156*, A169–A175.
- (42) Fuller, C. S.; Severiens, J. C. *Phys. Rev.* **1954**, *96*, 21–24.
- (43) Bodnarchuk, M. I.; Kravchyk, K. V.; Krumeich, F.; Wang, S.; Kovalenko, M. V. *ACS Nano* **2014**, *8*, 2360–2368.
- (44) Park, C.-M.; Kim, J.-H.; Kim, H.; Sohn, H.-J. *Chem. Soc. Rev.* **2010**, *39*, 3115–3141.
- (45) (a) Hewitt, K. C.; Beaulieu, L. Y.; Dahn, J. R. *J. Electrochem. Soc.* **2001**, *148*, A402–A410. (b) Wang, J.; Raistrick, I. D.; Huggins, R. A. *J. Electrochem. Soc.* **1986**, *133*, 457–460.
- (46) Darwiche, A.; Marino, C.; Sougrati, M. T.; Fraisse, B.; Stievano, L.; Monconduit, L. *J. Am. Chem. Soc.* **2012**, *134*, 20805–20811.
- (47) Heß, M.; Novák, P. *Electrochim. Acta* **2013**, *106*, 149–158.
- (48) Nakahara, K.; Nakajima, R.; Matsushima, T.; Majima, H. *J. Power Sources* **2003**, *117*, 131–136.
- (49) Murugesan, S.; Harris, J. T.; Korgel, B. A.; Stevenson, K. J. *Chem. Mater.* **2012**, *24*, 1306–1315.
- (50) Song, T.; Hu, L.; Paik, U. *J. Phys. Chem. Lett.* **2014**, *5*, 720–731.
- (51) Bogart, T. D.; Oka, D.; Lu, X.; Gu, M.; Wang, C.; Korgel, B. A. *ACS Nano* **2014**, *8*, 915–922.
- (52) Hanrath, T.; Korgel, B. A. *Adv. Mater.* **2003**, *15*, 437–440.
- (53) (a) Koo, B.; Xiong, H.; Slater, M. D.; Prakapenka, V. B.; Balasubramanian, M.; Podsiadlo, P.; Johnson, C. S.; Rajh, T.; Shevchenko, E. V. *Nano Lett.* **2012**, *12*, 2429–2435. (b) Koo, B.; Chattopadhyay, S.; Shibata, T.; Prakapenka, V. B.; Johnson, C. S.; Rajh, T.; Shevchenko, E. V. *Chem. Mater.* **2013**, *25*, 245–252. (c) Oh, M. H.; Yu, T.; Yu, S.-H.; Lim, B.; Ko, K.-T.; Willinger, M.-G.; Seo, D.-H.; Kim, B. H.; Cho, M. G.; Park, J.-H.; Kang, K.; Sung, Y.-E.; Pinna, N.; Hyeon, T. *Science* **2013**, *340*, 964–968. (d) Wang, Z.; Lou, X. W. *Adv. Mater.* **2012**, *24*, 4124–4129. (e) Jia, X.; Chen, Z.; Cui, X.; Peng, Y.; Wang, X.; Wang, G.; Wei, F.; Lu, Y. *ACS Nano* **2012**, *6*, 9911–9919. (f) Wang, D.-S.; Xie, T.; Peng, Q.; Zhang, S.-Y.; Chen, J.; Li, Y.-D. *Chem.—Eur. J.* **2008**, *14*, 2507–2513. (g) Ha, D.-H.; Islam, M. A.; Robinson, R. D. *Nano Lett.* **2012**, *12*, 5122–5130. (h) Liu, J.; Zhou, Y.; Liu, F.; Liu, C.; Wang, J.; Pan, Y.; Xue, D. *RSC Adv.* **2012**, *2*, 2262–2265. (i) Choi, C. S.; Park, Y.-U.; Kim, H.; Kim, N. R.; Kang, K.; Lee, H. M. *Electrochim. Acta* **2012**, *70*, 98–104. (j) Bresser, D.; Paillard, E.; Binetti, E.; Krueger, S.; Striccoli, M.; Winter, M.; Passerini, S. *J. Power Sources* **2012**, *206*, 301–309. (k) Ming, J.; Park, J.-B.; Sun, Y.-K. *ACS Appl. Mater. Interfaces* **2013**, *5*, 2133–2136. (l) Li, W.; Wang, F.; Feng, S.; Wang, J.; Sun, Z.; Li, B.; Li, Y.; Yang, J.; Elzatahry, A. A.; Xia, Y.; Zhao, D. *J. Am. Chem. Soc.* **2013**, *135*, 18300–18303. (m) Jin, Y.-H.; Seo, S.-D.; Shim, H.-W.; Park, K.-S.; Kim, D.-W. *Nanotechnology* **2012**, *23*, 125402. (n) Cheng, F.; Huang, K.; Liu, S.; Liu, J.; Deng, R. *Electrochim. Acta* **2011**, *56*, 5593–5598.
- (54) (a) Kwon, N. H.; Fromm, K. M. *Electrochim. Acta* **2012**, *69*, 38–44. (b) Rangappa, D.; Sone, K.; Zhou, Y.; Kudo, T.; Honma, I. *J. Mater. Chem.* **2011**, *21*, 15813–15818. (c) Doi, T.; Yatomi, S.; Kida, T.; Okada, S.; Yamaki, J.-i. *Cryst. Growth Des.* **2009**, *9*, 4990–4992.
- (55) Tarascon, J.-M. *Philos. Trans. R. Soc. A* **2010**, *368*, 3227–3241.
- (56) Supran, G. J.; Shirasaki, Y.; Song, K. W.; Caruge, J.-M.; Kazlas, P. T.; Coe-Sullivan, S.; Andrew, T. L.; Bawendi, M. G.; Bulovic, V. *MRS Bull.* **2013**, *38*, 703–711.
- (57) Myung, S.-T.; Noh, H.-J.; Yoon, S.-J.; Lee, E.-J.; Sun, Y.-K. *J. Phys. Chem. Lett.* **2014**, *5*, 671–679.
- (58) Thackeray, M. M.; Kang, S.-H.; Johnson, C. S.; Vaughey, J. T.; Benedeka, R.; Hackney, S. A. *J. Mater. Chem.* **2007**, *17*, 3112–3125.